Divertor Erosion in DIII-D

D.G. Whyte[1], R. Bastasz[2], J.N. Brooks[3], W.R. Wampler[2], W.P. West[4], C.P.C. Wong[4]

1. UCSD, San Diego, CA, USA

2. Sandia National Laboratory, Albuquerque, NM, USA

3. Argonne National Laboratory, IL, USA

4. General Atomics, San Diego, CA

Abstract

Net erosion rates of carbon target plates have been measured in situ for the DIII-D lower divertor. The principal method of obtaining this data is the DiMES sample probe. Recent experiments have focussed on erosion at the outer strike-point of two divertor plasma conditions: 1) Attached ($T_e > 40$ eV) ELMing plasmas and 2) Detached ($T_e < 2$ eV) ELMing plasmas. The erosion rates for the attached cases are > 10 cm/year, even with incident heat flux < 1 MW/m^2. In this case, measurements and modeling agree for both gross and net carbon erosion, showing the near-surface transport and redeposition of the carbon is well understood and that effective sputtering yields are > 10%. In ELM-free discharges, this erosion rate can account for the rate of carbon accumulation in the core plasma. Divertor plasma detachment eliminates physical sputtering, while spectroscopically measured chemical erosion yields are also found to be low ($Y(C/D^+) \leq 2.0 \times 10^{-3}$). This leads to suppression of net erosion at the outer strike-point, which becomes a region of net redeposition (~ 4 cm/year). The private flux wall is measured to be a region of net redeposition with dense, high neutral pressure, attached divertor plasmas. Leading edges intercepting parallel heat flux (~50 MW/m^2) have very high net erosion rates (~ 10 μm/s) at the OSP of an attached plasma. Leading edge erosion, and subsequent carbon redeposition, caused by tile gaps can account for half of the deuterium codeposition in the DIII-D divertor.

Sandia is a multiprogram laboratory operated by Sandia Corporation, a Lockheed Martin Company, for the United States Department of Energy under contract DE-AC04-94AL85000.

1. Introduction

Net erosion of plasma facing materials (PFM) is one of the most important problems to solve in designing power producing magnetic confinement devices (tokamaks, stellarators, etc.). In tokamaks, the inherent poloidal asymmetry in plasma-material interactions (PMI) caused by the use of poloidal divertors concentrates particle flux, and therefore the regions of wall erosion outflux, onto a relatively small surface. High *net* erosion rates will lead to two or three operating limits in a steady-state device:

1) Plate lifetime, determined by the peak rate of net erosion.

2) Codeposited tritium inventory limits (for safety and fuel inventory) found in regions of net redeposition is determined by the poloidally integrated net erosion rate.

3) Core plasma impurity contamination, which limits power output due to fuel dilution and radiation losses, is also driven by the poloidally intergrated net erosion.

However, because the first two issues stated are of no concern in short pulse, present day machines, dedicated experiments to study and control net erosion have been less common that experiments dealing with wall "conditioning" (e.g. reducing PFM gas recycling, etc.) and plasma impurity contamination.

Laboratory and tokamak erosion experiments have mostly focussed on obtaining physical and chemical sputtering yields for candidate materials, but these yields only address a portion of the net erosion problem, since it is strongly affected by the redeposition and transport of the materials. This redeposition is mostly determined by the incident plasma properties (e.g. mean free path of ionization). The net erosion is further complicated by the redeposition back to the material leading to highly efficient self-sputtering. Finally, the 2-D transport of the impurities in the tokamak core /SOL play a role in the poloidal "re-arrangement" of impurities, and hence in the net erosion. These phenomena interact in a complex manner, making in situ measurements of net erosion necessary.

This paper will describe a campaign to measure the net erosion /redeposition rates in the divertor of the DIII-D tokamak under several operational conditions. The principal

DISCLAIMER

tool for this study is the DiMES sample probe [1]. Dedicated experiments are designed to carefully control and diagnose the sample exposure to allow comparisons between the sample's net erosion measurements, other erosion measurements (e.g. spectroscopy for gross erosion), the core plasma's impurity concentration and modeling of the erosion. It will be shown that: typical divertor net erosion rates in DIII-D would be unacceptable in a steady-state devices (> 10 cm/year), outer strike-point (OSP) net erosion can account for the source of carbon that accumulates in a low density/recycling ELM-free discharge, "leading edges" of PFMs have very high net erosion rates and contribute significantly to hydrogenic codeposition. Preliminary results show that divertor "detachment" eliminates the carbon net erosion and reduces the heat flux a factor of 5-10 at the OSP compared to an attached divertor with the same input power.

2. Experiments

The experimental method for measuring net erosion with DiMES has been previously described [2,3] and is briefly described here. A graphite sample is inserted whose surface is flush to the tiles of the DIII-D lower divertor, which are also graphite (ATJ), making the sample a part of the floor. The divertor plasma geometry and outer strike-point (OSP) position is controlled during the discharge to expose the 50 mm diameter DiMES sample only to steady-state divertor plasma conditions. Samples are exposed to several discharges (typical total exposure is 10-20 seconds). Identical non-exposure discharges with slow radial sweeps of the OSP provide detailed radial profiles of divertor plasma parameters (electron density and temperature (ne, Te), ion flux (Γi), tile temperature, incident heat flux (q), etc.). Pre and post-exposure ion beam analysis (IBA) of the Si depth marker implanted in the graphite samples determined net erosion/deposition to $\pm$ 10 nm [4].

2.1 Net and gross erosion rates: low power, attached OSP

The OSP region net erosion has been studied in two case of low recycling, low density divertor plasmas: *1*) ELM-free H-mode, *2*) ELMy H-mode. The plasma

parameters for these discharges are: $P_{inj} \sim 2.5 - 3$ MW, $I_p \sim 1.4$ MA, $n_{e,OSP} \sim 1.2 \times 10^{19}$ m^{-3}, $T_{e,OSP} \sim 45$-70 eV, $\Gamma_i \sim 3 \times 10^{23}$ $s^{-1}m^{-2}$, $q \sim 0.7$ MW·m^{-2}, field line angle of incidence, $\theta \sim 2°$. As previously reported [5,6] the peak net erosion rate was V_{net} =3.6 +/- 0.7 nm/s for Case 1, and V_{net} =3.0 +/- 0.7 nm/s for Case 2 *(Note: 1 nm/s ~ 3 cm/year ~ 1×10^{20} $m^{-2}s^{-1}$ for carbon with atomic concentration, $n_c \sim 1 \times 10^{29}$ m^{-3})*. The quantity and features of net erosion have been modeled using the WBC/REDEP [7,8] erosion code simulations.

An absolutely calibrated CCD camera, equipped with an interference filter, measures the radial profile of the brightness, B, (photons $s^{-1}m^{-2}sr^{-1}$) of a C^{+1} (CII - 5140 Å) spectral line for Case 1 (Fig. 1). Using the collisional-radiative (CR) excitation model from [9] and recommended ionization rates [10], the ionization/photon ratio (SXB) is calculated for the experimental T_e and n_e profiles. Assuming that all C^{+1} ions are ionized in the field of view (poloidal ionization mean free path, MFP < 10 mm at OSP), then $4\pi \cdot B \cdot SXB$ gives the gross carbon influx into the divertor plasma. Results shows that near the OSP the measured carbon influx matches REDEP modeling that includes oblique incidence and self-sputtering. The effective sputtering yield (Y_{eff} = carbon outflux / incident particle flux) is 10-20%, about four times larger than would be expected with normal incidence D, and no self-sputtering [5]. This results also shows that physical sputtering dominates over chemical sputtering (T_{plate} ~ 100°C, Y_{chem} ~1-2 %) for these high plasma temperature, low flux divertor regime. The SXB technique is questionable for $T_e < 10$ eV (i.e. 30-40 mm from OSP), because the ionization MFP becomes too long (see relative error in Fig. 1).

The fact that models and experiment agree for both the gross and net erosion gives greater confidence that the model is correctly treating the near surface transport of the sputtered carbon. The sputtered carbon apparently has a prompt (or local) redeposition efficiency $\geq$ 80-85% near the OSP (from ratios of net to gross erosion). The modeling has also supported the experimental observation that ELMs played a minor role in the time averaged erosion rates for these cases, principally because of the ELM's short duration (0.5 ms) and low duty factor (~3%).

2.2 *Core plasma carbon accumulation in ELM-free plasmas*

In Case 1 described above, the net loss rate of carbon from the OSP region can be calculated using: the measured net erosion rate (V_e), the width of the net erosion region ($\Delta R_e \sim 0.02$ m), the carbon atomic concentration ($n_C \sim 1.2\times10^{29}$ m^{-3}) and the assumption of toroidal symmetry for the erosion (at the DiMES radial location of R=1.48 m). Note that the erosion is toroidally uniform on the plasma-facing portion of the DiMES sample [3]). This gives $dN_{carbon}/dt = V_e\, \Delta r\, 2\pi R\, n_c \sim 7\times10^{19} \pm 1.5$ s^{-1} and a corresponding contribution to the electron inventory from ionization of $Z_{(=6)}\cdot dN_{carbon}/dt \sim 4.2\times10^{20} \pm 1.0$ s^{-1}. The inventory of electrons in the core plasma is measured by Thomson scattering and the carbon inventory is measured by multi-chord charge exchange recombination (CER) spectroscopy [2,11]. The initial rapid increase in density particle confinement and density during the ELM-free phase is caused by the higher particle confinement time of the ELM-free period (Fig. 2). After 200 ms the density increases linearly with time. This increase is mostly due to the increasing carbon inventory in the core plasma, which is contributing Z=6 electrons for each carbon ion. The constant carbon source rate from the OSP region can account for the majority of this carbon accumulation rate, and hence the lack of density control, in the core plasma during the ELM-free period. Of course, this is not conclusive proof that the carbon in the core is from the OSP, since other poloidal location's net erosion is not measured. However, the fact that the carbon ions leave the OSP region as ions, near the separatrix, supports the idea that they would transport into the core SOL and eventually into the core plasma. This interpretation is supported by preliminary results from 1-D and 2-D modeling of DIII-D [12-14]. Their results suggest that thermal gradient forces would be larger than frictional forces in the OSP region. This exerts a net force away from the divertor plate (as opposed to frictional forces that tend to push the ions toward the plate) on the carbon ions that reside 10-20 mm's poloidal distance off the plate.

2.3 *OSP net erosion: Attached vs. detached plasmas*

The use of divertor detachment in reducing the heat flux to the divertor plates is well established on DIII-D [15] and elsewhere [16]. A set of experiments was performed to assess the effect of divertor detachment on carbon net erosion rates at the OSP. The OSP net erosion was measured in plasma discharges with identical injected power ($P_{inj} \sim 7$ MW) , plasma current ($I_p \sim 1.4$ MA), geometry (single lower divertor, no pumping) and confinement (ELMy H-mode, stored energy ~ 1 MJ). In the detached case, a programmed D_2 gas injection (~ 100 Torr-l/s) was used to increase the plasma density to $n_e \sim 1\times10^{20}$ m^{-3} from its "natural" value of $n_e \sim 4\times10^{19}$ m^{-3} in the attached case. The resulting differences in the OSP plasma parameters are shown in Fig. 3. The detached case shows the typical signatures of "radiative divertor" experiments in DIII-D [17], with $T_{e,plate}$ ~1-2 eV (measured with divertor Thomson scattering, DTS)over the entire OSP region, a radial "spreading out" of the incident ion flux (with the peak ion flux appearing outboard from the OSP) and a 5-10 fold reduction in the heat flux at the OSP. The incident neutral flux (Γ_0) is an order of magnitude larger than the ion flux at $\sim 4\times10^{23}$ s^{-1} m^{-2} (as measured by a divertor pressure gauge, see 2.4) assuming an incident energy of 2 eV for the neutrals (dissociation energies, T_i). The neutral flux can be assumed to be fairly spatially uniform due to the long MFP of ionization for D neutrals.

The attached case shows a toroidal pattern of deposition/erosion similar to those previously reported at these plasma conditions (i.e. attached, 2 MW/m^2). The cause of this pattern was speculated to be a toroidally localized, enhanced erosion source caused by a 0.1 mm height misalignment between the DiMES sample and the toroidally adjacent (downstream) tile. However, the misalignment was rectified for the current experiment The DiMES sample was placed in a rooftop style alignment, with the toroidally adjacent tiles being ~ 0.5 mm higher (upstream) and 0.5 mm lower (downstream). The persistence of the pattern (although the quantity of redeposition is reduced with the new alignment) suggests that ELMs are the principal cause of the localized erosion source via ablation at the tile gap (~3-5 mm) between the sample and the downstream tile (see 2.5 for details). Nevertheless, the radial profile of the minimum erosion rate for the flat surface (Fig. 3) can be measured at the toroidal location on the sample where the least "interference" from the localized source is expected. This toroidal position (about 10 mm upstream

from the center) is the furthest away from the downstream tile, yet not in the region shadowed by the upstream tile (which is also a region of net redeposition [6,18]) or the metal films. This shows that the peak net erosion rate is ~ 10 –12 nm/s for the carbon just inboard of the OSP in the attached case.

In the detached case the *OSP net erosion is eliminated and the OSP becomes a region of net redeposition*, with the build-up rate being ~1.5 nm/s (Fig. 3). As opposed to the attached case the redeposition exhibits toroidal uniformity on the sample. At these cold plasma temperatures and incident particle energies, chemical sputtering is the only expected source of erosion (i.e. $Y_{chem} \leq 10^{-2} \gg Y_{physical} \sim 0$) [19,20]. Therefore, it is useful to examine the expected and measured chemical erosion rates and their impact on the sample erosion.

Surprisingly, there is weak experimental evidence of chemical erosion occurring at the OSP. The upper limits on the expected chemical sputtering yield of the target can be estimated from two methods: comparisons of expected and measured redeposition, and hydrocarbon molecular spectroscopy. The results are summarized in Table 1.

The minimum expected redeposition rate from sources external to the divertor can be estimated from the core concentration of carbon as measured by CER (f_C =0.015 at r/a > 0.8). Carbon ions transported along the SOL from the core will begin to be "depleted" via recombination to the neutral state when $T_e \leq 2.5$ eV (i.e. $S_{ion} < S_{rec}$). For the detached case this occurs ~ 0.1 m poloidal distance from the plate. Measurements show that at the separatrix ~ 80% of the ion flux recombines through this region. Therefore, one expects the vast majority of this "external" carbon to impinge as neutrals at the divertor plate (since carbon recombines more efficiently that deuterium at these temperatures). Using the DTS measured ion flux above the recombining plasma of ~ 1.0×10^{23} s^{-1} m^{-2} at the separatrix and f_C, gives Γ_C ~1.5×10^{21} $s^{-1}m^{-2}$. This carbon ion flux is "re-distributed" to the floor due to their roughly isotropic spatial distribution after recombination. The flux to the sample's 50 mm width (using the flux surface and outer divertor geometries) is reduced a factor ~ 6-12 (compared to the upstream flux), giving an expected carbon

deposition rate of 1.2 - 2.5×10^{20} s^{-1} m^{-2} or ~ 1.2 - 2.5 nm/s. This implies that the local (divertor) net erosion contribution is < 1 nm/s (expected redeposition minus the measured redeposition) from the inboard side of the sample to the OSP and < 2 nm/s at the furthest outboard point on the sample. Including the preliminary result [21] that the prompt redeposition efficiency R is ~ 89% and the measured incident ion flux (3.0×10^{23} s^{-1} m^{-2}) and neutral flux (4.0×10^{24} s^{-1} m^{-2}) at the target gives an upper limit (i.e. $Y < \Gamma_{net,max}/\Gamma_{incident}/(1-R)$) on the expected sputtering yield (Table 1 shows the results for < 1nm/s). Note that this includes the effect of higher order hydrocarbons than methane (CD_4) such as C_2D_4 etc

An absolutely calibrated spectrometer, directly viewing (Fig. 4) the DiMES sample (and other divertor locations) found that the CD radical (4308 Å, $A^2\Delta - X^2\Pi$) band was everywhere below the "limit of detection" brightness ($B_{CD} < 1.5\times10^{16}$ photons s^{-1} m^{-2} sr^{-1}). It is noted that the 4300 Å band has been positively identified under other plasma conditions. The transport and break-up sequence of hydrocarbon molecules is modeled using WBC [21]. At these low T_e, the molecular ionization and dissociation are dominated by hydrocarbon-deuteron charge exchange (CX: $CD_y + D^+ \rightarrow CD_y^+ + D$) and dissociative recombination (DR: $CD_y^+ + e \rightarrow CD_{y-1} + D^+$). The models show that ~ 50% of the carbon released as hydrocarbons OSP wall will dissociate through the CD radical state. Previous measurements of the dissociations (or molecules) per photons (DXB) for the CD 4300 Å band gave DXB ~ 100 at T_e~10 eV for methane injection [22], in which case all the molecules will dissociate through the CH phase. Therefore, this rate is adjusted to reflect the 50% CD state probability from the modeling in order to give DXB (molecules/ $CD_{4300Å}$ photon) ~ 200. There is a concern for the validity of this rate at the low T_e ~ 1-2 eV found in the detached plasma. However, at Te~10 eV, the CX and DR rates are roughly double the dissociation / ionization rates via electron impact collision [23,24] and would dominate the break-up and excitation process in [22]. Indeed, the measured DXB has a very weak T_e dependence below 20 eV. Therefore, the spectroscopic upper limit on carbon out-flux from the plate is $\Gamma_{Carbon} < 4\pi\cdot B\ DXB \sim 4.0\times10^{19}$ m^{-2} s^{-1}. This method shows that chemical erosion yields are $Y_{chem} \leq 10^{-3}$, similar

to results from Method 1. The spectroscopic results are the more certain of the two methods, since they do not rely on assumptions about redeposition sources or efficiency. The C_2 Swan band (5170 Å) is also below the detection limit, although its excitation efficiency is 0.25-0.5 of the CD band, even for C_2H_4 [22], making it a less sensitive gauge of chemical erosion. From [19], the expected sputtering yield (at 10 eV, $T_{surface}$ ~ 350 °K, $\Gamma_{D+} = 3\times10^{18}$ $m^{-2}s^{-1}$) for methane is $Y(CD_4/D^+) \sim 4.5\times10^{-3}$, and the total hydrocarbon yield is $Y(C/D^+) \sim 1\times10^{-2}$. If the recommended flux dependence of $\Gamma^{-0.1}$ is taken into account, the total yield would be expected to fall to ~ 5×10^{-3}. It is noted that in our experiment incident ion energies are lower than the lowest energy measured using ion beam techniques.

Sputtering yield assumptions	**Method 1 Expected redeposition**	**Method 2 CD spectroscopy**
Ions only	**< 3.6 x 10^{-3} / 0**	**< 1.2 x 10^{-3} / 0**
Ions = neutral	**< 2.5 x 10^{-4}**	**< 8 x 10^{-5}**
Ions, $Y_{neutral} = 10^{-4}$	**< 2.4 x 10^{-3} / 1.0 x 10-4**	**0 / 1.0 x 10-4**

Table 1 Upper limit on total chemical sputtering yields (ion / neutrals) from the detached OSP erosion experiment.

In the attached case, a 100 nm thick tungsten (W) film (3 mm toroidal extent) shows a significant erosion rate (~ 2 nm/s) outboard of the OSP and is apparently caused by arcing. The W erosion is co-incident with the radial presence of the arc tracks on the W film [6]. Also, the post-exposure changes in the Rutherford backscattering spectra off of the W are consistent with the removal of the entire thickness of the W over a fraction of the film's surface area (presumably caused by the arcs) rather than a uniform reduction in thickness that would be caused by "normal" sputtering. No arc tracks were found on the W film after the detached plasma exposure. Tungsten erosion was smaller than measurement uncertainty (< 0.07 nm/s) in the detached case, consistent with the expectation that no physical (or chemical) sputtering will occur for the tungsten for these low incident energies [25]. It is of interest to note that even the presence of type 1 ELMs ($q > 20$ MW/m^2, 0.5 ms duration), which have been shown to "burn" through the cold

detached plasma [26] to the floor (i.e. the incident heat flux per ELM is the same for attached plasmas), do not cause appreciable W erosion.

2.4 Private flux erosion

The PFM that resides in the private flux (PF) region of the divertor is of interest in erosion and impurity studies. Although plasma flux to this wall region is weak compared to the strike-points, it represents a comparatively large surface area. Incident particle distribution is mostly dissociated hydrogenic neutrals (incident energy, E_i ~1- 2 eV) and charge exchange neutral flux (E_i > 10 eV) from the X-point and divertor leg plasma. Sputtered carbon from the PF has better geometric access to the X-point region, and therefore could play an important role in determining the carbon content of the core plasma.

A depth marked graphite DiMES sample was exposed for 28 seconds (~300 °K surface temperature) in the PF region during a radiative divertor experiment on DIII-D. These lower single-null discharges (P_{inj} ~ 8MW) have the OSP placed at the lower pump entrance (R~1.68 m) and a large D2 gas injection (> 200 Torr L/s) at the midplane, in order to induce SOL flow. This is meant to enhance divertor compression of argon gas that is injected into the divertor through the PF region. This results in a highly radiative (P_{div} ~ 5 MW/m^3) and dense (outer divertor separatrix density ~ 5 –10 ×10^{19} m^{-3}) attached outer divertor. The sample (R=1.48 m) is 0.2 m from either strike-point and is located 0.2 m below the X-point (Fig. 4). A fixed position Langmuir probe provides the plasma parameters at the sample: n_e ~ 2.0×10^{18} m^{-3}, T_e = 2-3 eV, Γ_i ~ 7×10^{20} m^{-2} s^{-1}.

The PF region is characterized by large neutral densities and fluxes as measured by two diagnostic methods. The first uses a manometer pressure gauge that samples the neutral influx into a vertical port situated at the DiMES radial location (at another toroidal location). By using the DEGAS simulation result [27,28] that the majority of PF pressure is due to dissociated deuterium atoms (E ~ 2 eV, from Franck-Condon dissociation of D_2), their flux to the floor can be derived from the average measured

pressure (P ~ 15 mTorr), to give $\Gamma_0 \propto P\, E^{-1/2} \sim 1.0 \pm 0.3 \times 10^{23}$ m^{-2} s^{-1}. The neutral flux emanating from the PF region is also proportional to the D_α brightness measured at the outer divertor leg (Fig. 4). The measured D_α brightness (~3×10^{20} photons s^{-1} m^{-2} sr^{-1}) is converted to incident flux using an ionization/photon (SXB) ratio of 40 ± 10 giving $\Gamma_0 = 4\pi \cdot B \cdot SXB \sim 1.5 \pm 0.4 \times 10^{23}$ m^{-2} s^{-1}. The SXB ratio is calculated using a CR atomic model [29] for the excitation and ionization rates and simulating the emissions from 2 eV incident deuterium neutrals along the line of sight using the plasma density and temperature profiles. The two techniques agree within uncertainties and both increase linearly when the D2 gas injection is increased. Therefore, the incident neutral flux to the sample is at least two orders of magnitude larger than the ion flux and the neutral density in the PF $n_{0,PF} > 5\times10^{19}$ m^{-3}.

IBA analysis of the Si depth marker indicates a radially uniform net redeposition ~ 24 ± 3 nm for the carbon. This is equivalent to a *net redeposition rate* ~ $7x10^{19}$ m^{-2} s^{-1}. Therefore, the PF wall is a net *sink* for carbon under these conditions. If one expected only net erosion caused by neutral chemical sputtering, the sensitivity of this experiment to chemical erosion yield is $Y < 2\times10^{-4}$. . It is useful to examine the fate of chemically sputtered hydrocarbons in the PF region. Thermal hydrocarbon will undergo charge exchange with the D^+ ($= n_e \sim 2\times10^{18}$ m^{-3}) at a rate of $\langle\sigma v\rangle \sim 1\times10^{-14}$ $m^3 s^{-1}$ [23], resulting in a MFP of ionization of 25 mm (< X-point height) in the PF region. These will rapidly undergo CX back to the neutral state due to the high background D neutral density ($n_0 \sim 5\times10^{19}$ m^{-3}) but with an isotropic spatial re-distribution caused by their gyro-motion as an ion. Therefore, one would roughly expect that at least half of the CH released from the PF wall will redeposit back to the PF wall and half will impinge on the divertor plasma, dissociate and radiate in the CD band (∴DXB ~ 200, see 2.3). The CD (4300 Å) molecular band brightness is below detection limit for the viewing chord looking at DiMES and intercepting the outer divertor leg (Fig. 4). This implies that the net chemical erosion flux leaving the PF must be < 4.0×10^{19} m^{-2} s^{-1} and that the effective chemical sputtering yield is Y(C/D) < $2\text{-}3\times10^{-4}$ for the incident neutrals at the PF wall. These upper limits are similar to values for thermally dissociated atomic hydrogen's chemical

sputtering on pyrolitic graphite [30] (Y ~ 0.5- 2×10^{-4} at 300 °K). It is interesting to note that the simultaneous bombardment of ions ($\Gamma_i/\Gamma_0 \sim 10^{-2}$, with $E_i \sim$ 10-15 eV) and higher energy charge-exchange neutrals in this experiment does not seem to lead to the large enhancement in Y_{chem} as reported in [30] (100 fold increase with $\Gamma_{Ar+}/\Gamma_H \sim$1.0e-3).

There are two possible sources for the redepositing carbon flux. A carbon fraction of 10% in the incident plasma would result in ~ 7.0×10^{19} m^{-2} s^{-1} carbon influx to the plate. This seems reasonable since previous studies of attached divertor plasmas on DIII-D have shown $f_{C,divetor} > 10\%$ [9] and effective physical sputtering yields at the OSP are >10% (see 2.1). The other possible source is redeposition of hyrdrocarbons resulting from higher chemical erosion out-flux near the strike-points (redeposition of chemically eroded hydrocarbons from the PF wall only reduces the net erosion, but cannot cause net redeposition). However, this source would result in a molecular flux into the divertor leg/X-point plasma due to the CX process previously described. Therefore, this source of redeposition is less likely but possible, since the flux limit of detection from CD band spectroscopy (4×10^{19} m^{-2} s^{-1}) is just less than the net redeposition rate (7×10^{19} m^{-2} s^{-1}).

The experiments measuring OSP erosion (Sec. 2.1, 2.3) keep the sample in the PF (~ 1.5 seconds of ohmic plasma per exposure shot) until steady-state divertor conditions are achieved. However, during these times the neutral and ion flux is 5 –10 times lower than in the PF erosion experiment describe above, resulting in a net redeposition rate < 0.1 nm/s, which is within the uncertainty of the OSP erosion results.

2.5 Leading edge erosion

The presence of leading edges (a PFM surface that intercepts parallel heat flux) is known to create impurity problems (e.g re-designed tile geometry for JET [31]). A DiMES sample with an 0.7 mm vertical lip was exposed to the OSP of an ELMing H-mode plasma ($P_{inj} \sim$ 7 MW, $T_{e,OSP} \sim$ 30 eV, $n_e \sim 5\times10^{19}$ m^{-3}, q ~ 2 MW/m^2, $\theta \sim 2°$) for 0.5 seconds in order to study dust production caused by erosion [32]. Parallel heat flux ~ 50 MW/m^2 wetted an area of 14 mm^2, which thermal analysis shows reached a temperature > 2300 °K. Redeposited carbon was collected on a recessed Si wafer (200 mm^2) facing the leading edge but receiving no plasma flux itself. IBA showed a uniform

carbonaceous, diamond-like film of ~ 0.5 μm depth. From the ratios of the exposed and collection areas, the *net erosion rate of the leading edge is ≥ 6 μm/s* (this neglects carbon deposition elsewhere on the sample). The deuterium/carbon ratio in the film is 12%, leading to a hydrogenic codeposition rate of 0.18 g s^{-1} per m^2 of wetted leading edge.

The 5 mm gaps between the divertor tiles of DIII-D behave similarly to the leading edge described above. With perfectly horizontal tile alignment, each gap presents a leading edge ~ .15 mm in height (θ ~ 2°), but in practice the alignment tolerance is ~ 0.4 mm. The side of the adjacent tile directly facees the leading edge and will collect redeposited carbon (and codeposition) in a manner similar to the silicon wafer. Taking an average strike-point (inner and outer) width of 40 mm, and with ~ 80 toroidal tiles, gives the area of leading edge in the DIII-D lower divertor to be ~ 0.5 - 1.0 $\times 10^{-3}$ m^2. Previous analysis of DIII-D lower divertor tiles (exposed to 2000 shots or ~ 5000 s) [33] showed that roughly 0.5 g of the total 1 g of codeposited deuterium in the lower divertor was found in the tile gaps. Using the DiMES measured codeposition rate and DIII-D leading edges predicts a codeposition rate of ~ 0.5-1 g. Therefore, the high erosion rate caused by leading edges is a plausible explanation for the high percentage of carbon and hydrogenic redeposits found in tile gaps.

3. Discussion

The suppressed net erosion at the OSP during divertor detachment is encouraging. However it should be noted that in the detached divertor, the peak in the ion flux is actually outboard of the OSP, and may be the region of net erosion at the outer divertor (as suggested by the trend of lower redeposition at the outboard side in Fig. 3). Future experiments will address this issue.

The consistently low chemical sputtering yields inferred from these experiments (by spectroscopy and erosion) could be due to a combination of factors: relatively cold plate temperatures (≤ 350 °K), efficient redeposition of hydrocarbons due to the sonic plasma flow directed to the plate in detached plasmas [34], and high flux ($Y \propto \Gamma^{\sim 0.1}$). The lack of experimentally measured CD (4300 Å) DXB ratios at low plasma temperatures

(Te < 10 eV) is also of concern, where unknown breakup mechanisms for the hydrocarbons may reduce the expected CD emission.

A summary of the OSP carbon erosion experiments is shown in Fig. 5. Apparently, carbon's net erosion rate consistently increases with the incident heat flux for attached plasma conditions. Note that even at modest q (< 1 MW/m2) the attached OSP has a net erosion rate that would seem unacceptable for a steady-state device (> 10 cm/year) since the typical plate thickness is ~ 1-3 cm for heat conduction. The erosion rates from a long term (9 month) exposure of lower divertor tiles [1] have been included. These have greater uncertainty due to lack of plasma consistency over so many discharges (~ 1400 lower diverted shot).

The presence of such a large erosion rates (and corresponding codeposition) at leading edges is also of concern. Rooftop alignment of tiles eliminates leading edges but leads to areas of large redeposition in shadowed areas, and decreases the effective divertor area. Operational experience in DIII-D has found that placing the OSP in new poloidal locations, or reversing the magnetic orientation (and hence finding "new" leading edges), leads to enhanced carbon impurities until sufficient "conditioning" of these edges occurs over several shots. This is consistent with the observation that the typical leading edge is ≥ 0.1 mm, and would erode at a rate ~ 0.01 mm/s (Section 2.5), therefore taking 10's of seconds (or several shots) to rectify.

4. Conclusion

Net erosion rates of carbon have been measured in the DIII-D divertor. The erosion rates at an attached OSP are > 10 cm/year, even with incident heat flux < 1 MW/m^2. In ELM-free discharges, this erosion rate can account for the rate of carbon accumulation in the core plasma. Divertor plasma detachment decreases the incident plasma temperature below 2 eV, and the subsequent elimination of physical sputtering suppresses net carbon erosion at the outer strike-point. Tungsten erosion is also eliminated during detached operations. The private flux wall is a region of net redeposition with dense, high neutral pressure attached plasmas. Leading edges have net

erosion ~ 10 mm/s at the OSP of an attached plasma. The erosion of leading edges caused by tile gaps can account for half of the codeposition in the DIII-D divertor.

Figure Captions

Fig. 1

Radial profiles of erosion in low power attached plasmas.
{Top} Measured plasma temperature and CII brightness and calculated ionization/photon ratio (SXB). {Middle{ Measured (light line and points)and REDEP predicted (dark line) gross (ELM-free case) and net (ELMy case) carbon erosion rates. {Bottom} Measured and REDEP predicted effective sputtering yield.

Fig. 2

{Top} Time traces of plasma density and D_α showing ELM-free period used for DiMES erosion measurements. {Bottom} Measured rate of change in core electron inventory during ELM-free phase and inferred source rate from core carbon inventory increase and OSP erosion rate. Each carbon atom contributes 6 electrons.

Fig. 3

Plasma parameters and carbon/tungsten erosion rates vs. radial position from OSP. Light line: attached plasma. Dark line: detached plasma. ($V_e < 0$ indicates erosion, $V_e > 0$ indicates net redeposition)

Fig. 4

Exposure geometry for DiMES experiments. Solid separatrix outline: OSP erosion experiments. Dashed separatrix outline: PF erosion experiments. Location of divertor spectrometer/D_α viewing chord and divertor Thomson scattering (DTS) is also shown.

Fig. 5

Net rate of change for carbon plate thickness (V_{carbon}) vs. peak incident heat flux, q for DiMES erosion experiments at the OSP.

References

[1] C. P. C. Wong, R. Junge, R. D. Phelps *et al.*, J. Nucl. Mater. **196-198** (1992) 871.

[2] D.G. Whyte, Wade M.R., Finkenthal, D.F., Burrell, K.H. , Monier-Garbet, P., Rice, B.W., Schissel, D.P., West, W.P., Wood, R.D., Nucl. Fusion (1998) to be published Feb. 1998.

[3] R. Bastasz, W. R. Wampler, J. W. Cuthbertson *et al.*, J. Nucl. Mater. **220-222** (1995) 310.

[4] W. R. Wampler, R. Bastasz, D. Buchenauer *et al.*, J. Nucl. Mater. **233** (1995) 791.

[5] J.N. Brooks and D.G. Whyte, Nucl. Fusion (1998) submitted for publication.

[6] D. G. Whyte, J. N. Brooks, C. P. C. Wong *et al.*, J. Nucl. Mater. **241-243** (1997) 660.

[7] J. N. Brooks, Nuclear Technology/Fusion **4** (1983) 33.

[8] N. J. Brooks, Physics of Fluids B (Plasma Physics) **2** (1990) 1858.

[9] R.C. Isler, Perosnal communication, DIII-D, San Diego, USA (1998).

[10] M. A. Lennon, K. L. Bell, H. B. Gilbody *et al.*, Journal of Physical and Chemical Reference Data **17** (1988) 1285.

[11] P. Gohil, K. H. Burrell, R. J. Groebner *et al.*, Rev. Sci. Instrum. **61** (1990) 2949.

[12] W. P. West, S. L. Allen, N. H. Brooks *et al.*, Plasma Physics and Controlled Fusion **39** (1997) 295.

[13] T. D. Rognlien, J. L. Milovich, M. E. Rensink *et al.*, J. Nucl. Mater. **196-198** (1992) 347.

[14] G.D. Porter, Personal Communication, DIII-D, San Diego, USA (1997).

[15] T. W. Petrie, D. N. Hill, S. L. Allen *et al.*, Nucl. Fusion **37** (1997) 321.

[16] G. F. Matthews, J. Nucl. Mater. **220-222** (1995) 104.

[17] M. E. Fenstermacher, R. D. Wood, S. L. Allen *et al.*, J. Nucl. Mater. **241-243** (1997) 666.

[18] J. P. Coad, M. Rubel, and C. H. Wu, J. Nucl. Mater. **241-243** (1997) 408.

[19] J. W. Davis and A. A. Haasz, J. Nucl. Mater. **241-243** (1997) 37.

[20] W. Eckstein, C. Garcia-Rosales, J. Roth *et al.*, "Sputtering Data," IPP, Garching, Germany, IPP 9/82, 1993.

[21] J.N. Brooks, D.N. Ruzics, and D.G. Whyte, Journal of Nuclear Material (1998).

[22] Y. Ra, A. Pospieszczyk, Y. Hirooka *et al.*, Journal of Vacuum Science & Technology A (Vacuum, Surfaces, and Films) **8** (1990) 1783.

[23] A.B. Ehrhardt and W.D. Langer, "Collisional processes of hydrocarbons in hydrogen plasmas," PPPL, Princeton, N.J., PPPL-2477, 1987.

[24] P. M. Mul, J. B. A. Mitchell, V. S. D'Angelo *et al.*, Journal of Physics B (Atomic and Molecular Physics) **14** (1981) 1353.

[25] J. N. Brooks, R. Causey, G. Federici *et al.*, J. Nucl. Mater. **241-243** (1997) 294.

[26] A.W. Leonard, G.D. Porter, R.D. Wood *et al.*, Plasma Physics (1998).

[27] M. E. Fenstermacher, G. D. Porter, M. E. Rensink *et al.*, J. Nucl. Mater. **220-222** (1995) 330.

[28] M.E. Fenstermacher, Personal communication, DIII-D, San Diego, USA (1998).

[29] H.P. Summers, "Atomic Data and Analysis Structure," JET Joint Undertaking, Abingdon, UK, 1994.

[30] E. Vietzke, K. Flaskamp, and V. Philipps, J. Nucl. Mater. **111-112** (1982) 763.

[31] D. J. Campbell, J. Nucl. Mater. **241-243** (1997) 379.

[32] O.I. Buzhinskij and et. al., J. Nucl. Mater. (1998).

[33] D. S. Walsh, B. L. Doyle, and G. L. Jackson, Journal of Vacuum Science & Technology A (Vacuum, Surfaces, and Films) **10** (1992) 1174.

[34] A. W. Leonard, M. A. Mahdavi, S. L. Allen *et al.*, Phys. Rev. Lett. **78** (1997) 4769.

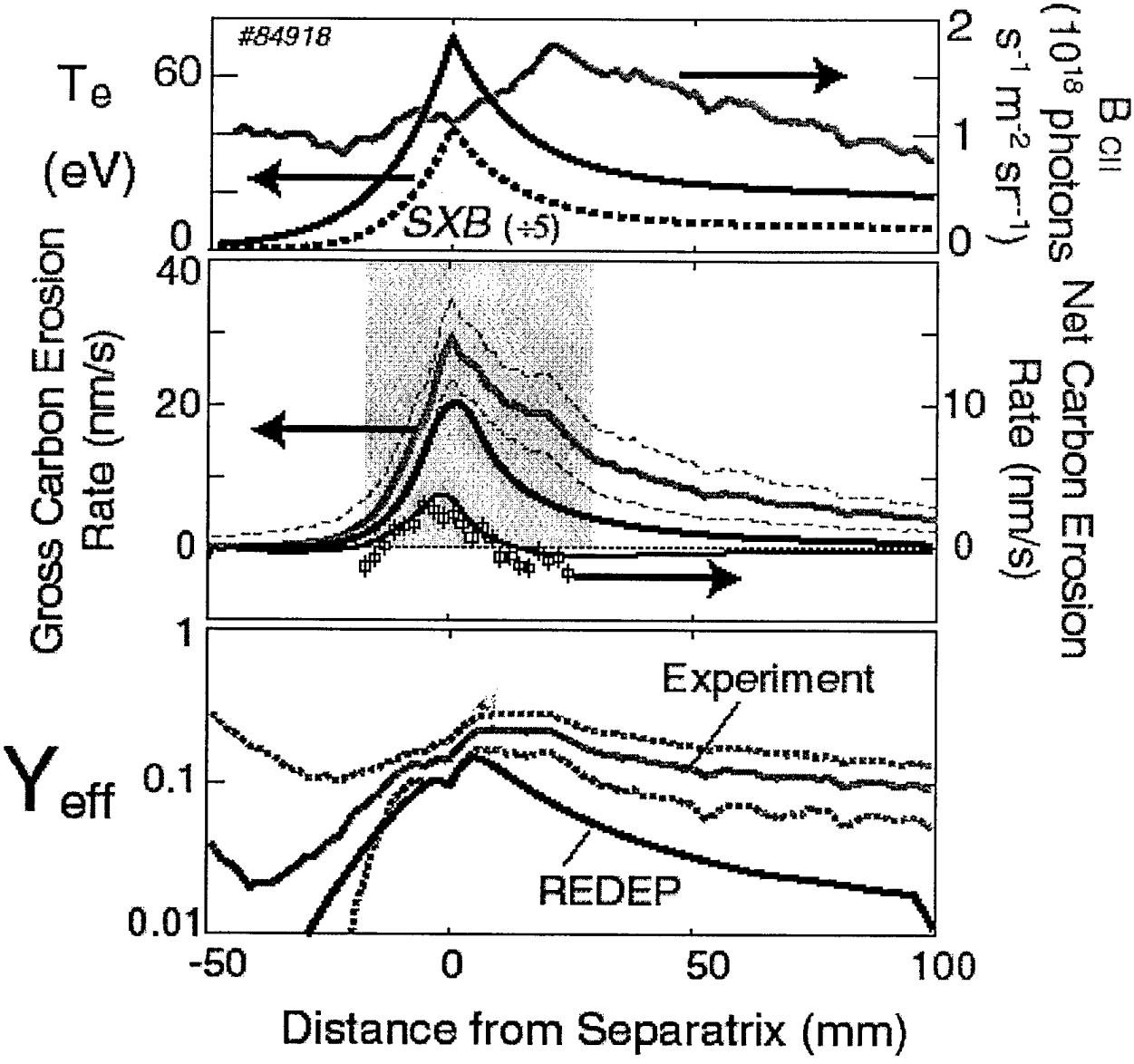
#84918
T_e (eV)
60
0
SXB (÷5)
2
1
0
B_{CII} (10^{18} photons s^{-1} m^{-2} sr^{-1})
Gross Carbon Erosion Rate (nm/s)
40
20
0
10
0
Net Carbon Erosion Rate (nm/s)
Y_{eff}
1
0.1
0.01
Experiment
REDEP
-50
0
50
100
Distance from Separatrix (mm)

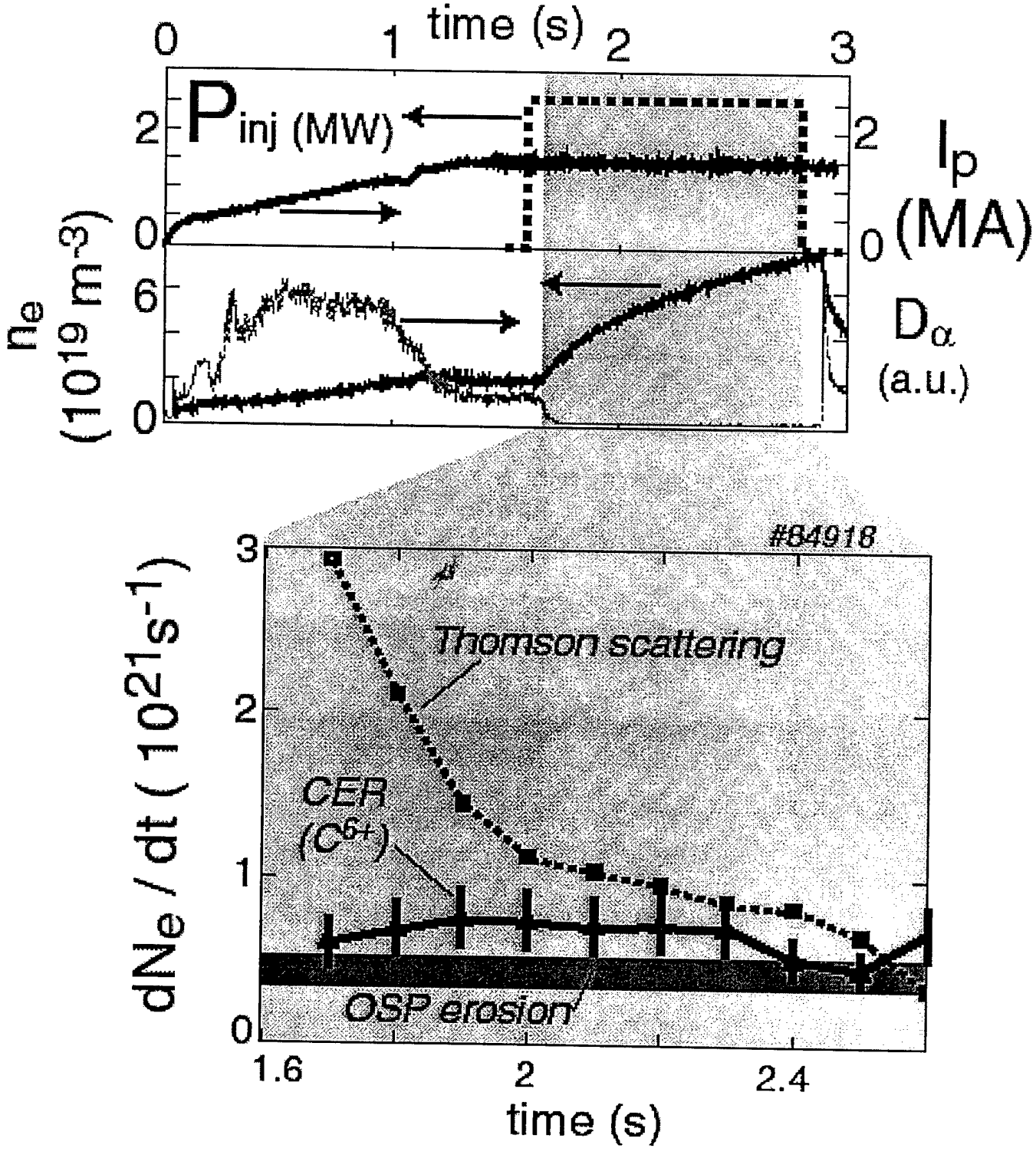
time (s)
0
1
2
3
P_{inj} (MW)
2
0
I_p (MA)
2
0
n_e (10^{19} m^{-3})
6
0
D_α (a.u.)
#84918
Thomson scattering
CER (C^{6+})
OSP erosion
dN_e / dt ($10^{21} s^{-1}$)
3
2
1
0
1.6
2
2.4
time (s)

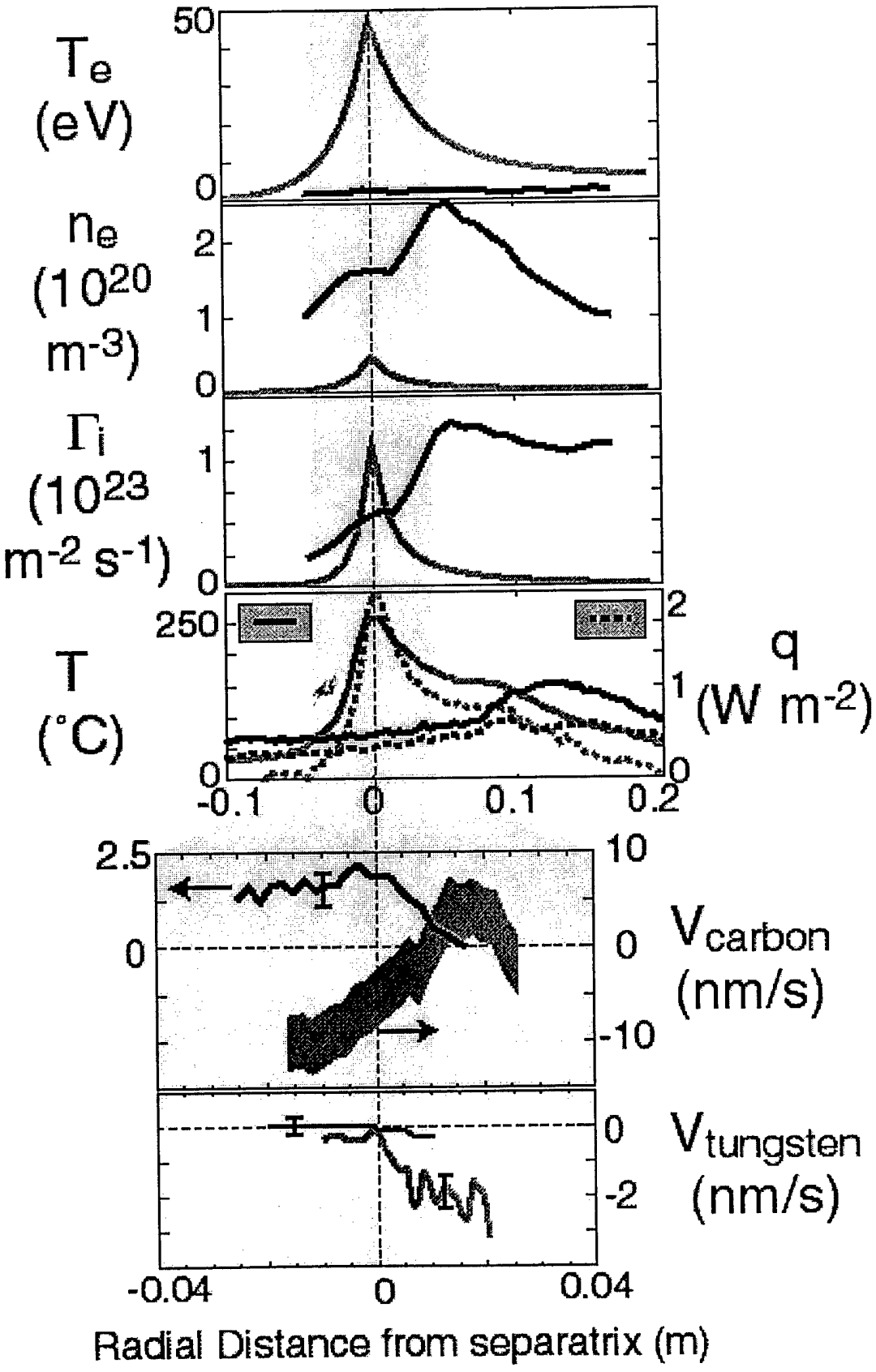
T_e (eV)
50
0
n_e (10^{20} m^{-3})
2
1
0
Γ_i (10^{23} m^{-2} s^{-1})
1
0
T (°C)
250
0
q (W m^{-2})
2
1
0
-0.1
0
0.1
0.2
2.5
0
10
0
-10
V_{carbon} (nm/s)
0
-2
$V_{tungsten}$ (nm/s)
-0.04
0
0.04
Radial Distance from separatrix (m)

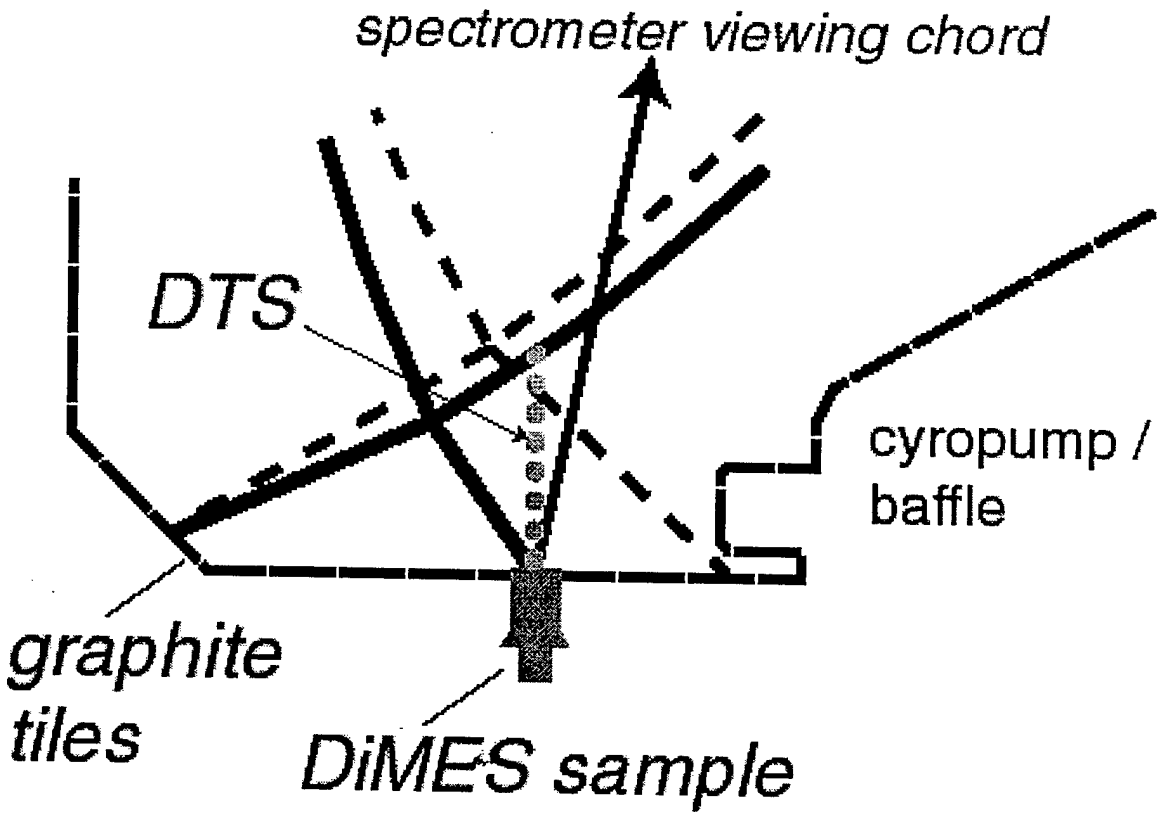
spectrometer viewing chord
DTS
cyropump /
baffle
graphite
tiles
DiMES sample

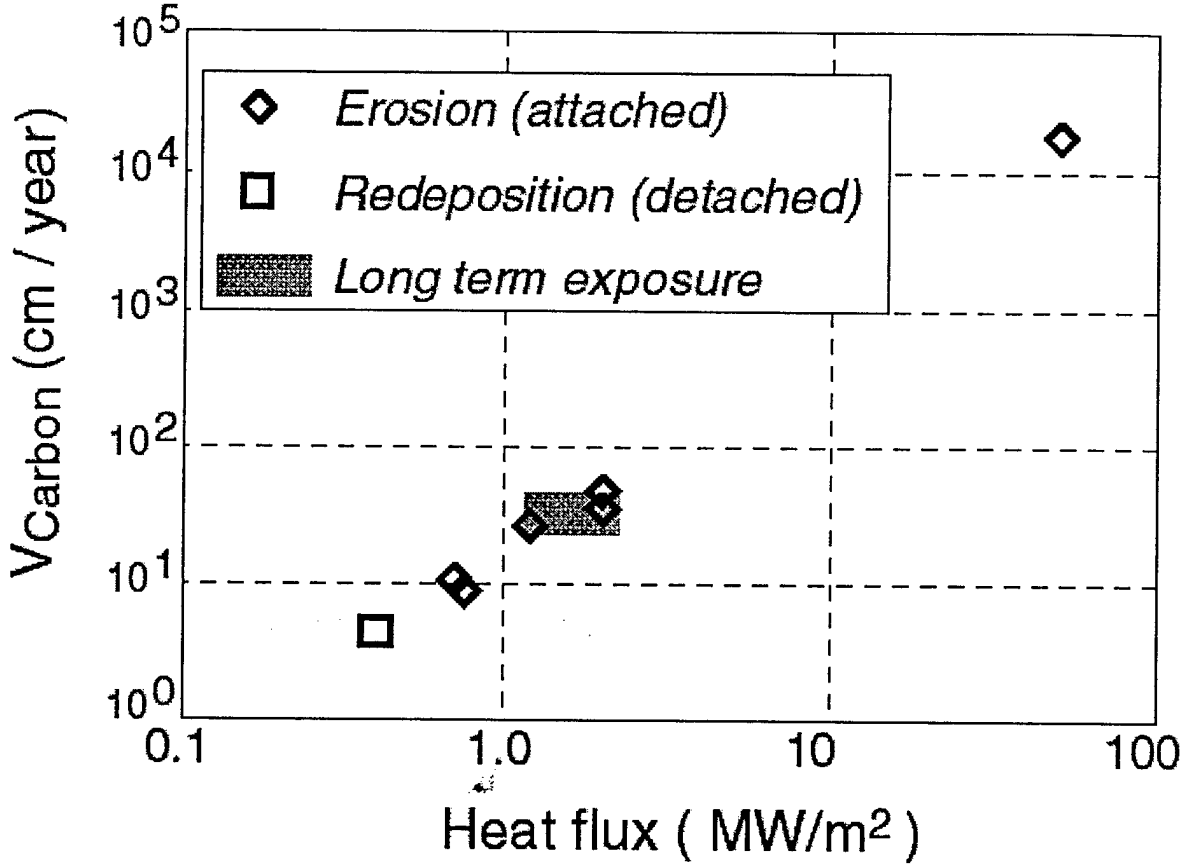
Erosion (attached)
Redeposition (detached)
Long term exposure
10^5
10^4
10^3
10^2
10^1
10^0
0.1
1.0
10
100
VCarbon (cm / year)
Heat flux (MW/m^2)

Report Number (14) SAND--98-0350
CONF-9805160-

Publ. Date (11) 05

Sponsor Code (18) DOE/ER, XF

UC Category (19) UC-423, DOE/ER

DOE